Radiation Effects & Defects in Solids, 2014 – http://dx.doi.org/10.1080/10420150.2014.988625

Unitary quantum lattice gas algorithm generated from the Dirac collision operator for 1D soliton-soliton collisions

Armen Oganesov[1], George Vahala[1], Linda Vahala[2],
Jeffrey Yepez[3,4], Min Soe[5] and Bo Zhang[6]
[1]*Department of Physics, William & Mary, Williamsburg, Virginia 23185*
[2]*Department of Electrical & Computer Engineering,*
Old Dominion University, Norfolk, VA 23529
[4]*Department of Physics and Astronomy,*
University of Hawai'i at Manoa Watanabe Hall,
2505 Correa Road, Honolulu, Hawai'i 96822
[5]*Department of Mathematics and Physical Sciences,*
Rogers State University, Claremore, OK 74017
[6]*Institute for Fusion Research, University of Texas, Austin, TX 78712*

Abstract

A new unitary quantum lattice gas (QLG) algorithm is proposed as a mesoscopic unitary perturbative representation of the mean field Gross Pitaevskii equation for Bose Einstein Condensates (BECs). This consists of an interleaved sequence of unitary collide-stream operators and is tested on the 1D nonlinear Schrodinger (NLS) equation since exact soliton solutions are well known. An earlier QLG algorithm, based on the $\sqrt{\text{SWAP}}$ collision operator has been found to have limited application to spinor-BECs. Here a new unitary collision operator, based on the recent QLG of Yepez for the Dirac particle, is used to model the 1D NLS soliton-soliton problem. It is found that this new unitary algorithm can handle parameters (soliton amplitudes and speeds) a factor of over 20 greater than those under the previous $\sqrt{\text{SWAP}}$ algorithm.

I. INTRODUCTION

Recently, a new computational paradigm has arisen due to the one of the most puzzling concepts of quantum mechanics—quantum entanglement [1]. This has led to a major interest in the field of quantum computation and quantum information theory whose basic building block is the qubit. Unlike the classical bit, which can only take on the value of "0" or "1", the qubit can reside in a general superposition state of the two (classical) states "0" and "1" with complex probability amplitudes α_0, α_1:

$$|q\rangle = \alpha_0|0\rangle + \alpha_1|1\rangle \qquad \text{with} \qquad |\alpha_0|^2 + |\alpha_1|^2 = 1. \tag{1}$$

Two qubits thus exist in a four-dimensional state (with corresponding normalization)

$$|q_1 q_2\rangle = \alpha_{00}|00\rangle + \alpha_{01}|01\rangle + \alpha_{10}|10\rangle + \alpha_{11}|11\rangle \tag{2}$$

The quantum informational approach of specifying quantum dynamics, which is originally due to Feynman [2, 3], is a rather new approach. The more traditional approach to quantum dynamics is through the Hamiltonian or Lagrangian.

The quantum lattice gas (QLG) is one of the earliest quantum algorithms devised [4–14]. If the local entangling gate structure (i.e. quantum algorithmic protocol) is chosen appropriately, then the flow of quantum information can emulate, in the long wavelength limit, a quantum wave function governed by an equation of motion such as the Weyl, Dirac, or Schroedinger wave equation [15]. The quantum lattice-gas representation constitutes a universal model of quantum computation. Further, any particular quantum lattice gas representation of a quantum system is a faithful representation. Here we focus on the effect of different representations of the one-dimensional nonlinear Schrdoinger equation (NLS) – in the particular choices of the unitary collision operators. A somewhat related alternate approach has been considered by Succi and his collaborators [16–18].

The NLS is an important equation of physics, arising in the study of Langmuir waves in plasmas, in nonlinear wave propagation in optical fibers, in energy transport along molecular chains, as well as the ground state dynamics of Bose-Einstein Condensates. In one dimension (1D), the NLS will permit exact soliton solutions. In particular, the exact 1-soliton solution to the 1D NLS equation

$$i\partial_t \Phi = -\partial_{xx}\Phi - |\Phi|^2\Phi, \tag{3}$$

is the 2-parameter family solution

$$\Phi(x,t) = a\sqrt{2}\,\exp\left[i\left(\frac{bx}{2} - \left(\frac{b^2}{4} - a^2\right)t\right)\right]\,\mathrm{sech}[a(x-bt)] \tag{4}$$

where $a\sqrt{2}$ is the soliton amplitude, and b is the soliton speed. When one moves to $3D$ there are no longer exact solutions. Some specific Pade approximate solutions have been determined by Berloff – but now there are no longer any free parameters in the solutions as in the 2-free parameters in 1D NLS.

QLG is a unitary mesoscopic algorithm with interleaved collision-stream operators: the local unitary collision operator entangles the qubit amplitudes while the unitary stream operator moves that entanglement throughout the lattice. We first considered the unitary collision matrix as the $\sqrt{\mathrm{SWAP}}$ gate with representation

$$C_{\sqrt{\mathrm{SWAP}}} = \begin{pmatrix} 1 & 0 & 0 & 0 \\ 0 & \frac{1}{2}+\frac{i}{2} & \frac{1}{2}-\frac{i}{2} & 0 \\ 0 & \frac{1}{2}-\frac{i}{2} & \frac{1}{2}+\frac{i}{2} & 0 \\ 0 & 0 & 0 & i \end{pmatrix} = \exp\left[i\frac{\pi}{2}\begin{pmatrix} 0 & 0 & 0 & 0 \\ 0 & \frac{1}{2} & -\frac{1}{2} & 0 \\ 0 & -\frac{1}{2} & \frac{1}{2} & 0 \\ 0 & 0 & 0 & 1 \end{pmatrix}\right], \tag{5}$$

in the basis

$$|00\rangle = \begin{pmatrix}1\\0\\0\\0\end{pmatrix}, \quad |01\rangle = \begin{pmatrix}0\\1\\0\\0\end{pmatrix}, \quad |10\rangle = \begin{pmatrix}0\\0\\1\\0\end{pmatrix}, \quad |11\rangle = \begin{pmatrix}0\\0\\0\\1\end{pmatrix}. \tag{6}$$

In the 1-body subspace $|01\rangle$, $|10\rangle$ of the 4D 2-qubit Hilbert space, the local unitary $\sqrt{\text{SWAP}}$ collision operator takes the form

$$C = \exp\left[i\frac{\pi}{4}\sigma_x(1-\sigma_x)\right] = \frac{1}{2}\begin{pmatrix}1-i & 1+i\\ 1+i & 1-i\end{pmatrix} = e^{i\frac{\pi}{4}}\begin{pmatrix}cos\,\theta_\circ & -i\,sin\,\theta_\circ\\ -i\,sin\,\theta_\circ & cos\,\theta_\circ\end{pmatrix}, \tag{7}$$

for $\theta_\circ = \pi/4$ and where the $\boldsymbol{\sigma}$ are the Pauli spin matrices

$$\sigma_x = \begin{pmatrix}0 & 1\\ 1 & 0\end{pmatrix} \qquad \sigma_y = \begin{pmatrix}0 & -i\\ i & 0\end{pmatrix} \qquad \sigma_z = \begin{pmatrix}1 & 0\\ 0 & -1\end{pmatrix}. \tag{8}$$

The corresponding wave function at lattice site $\boldsymbol{x}$

$$\psi(\boldsymbol{x},t) = \begin{pmatrix}\alpha_{01}(\boldsymbol{x},t)\\ \alpha_{10}(\boldsymbol{x},t)\end{pmatrix} \tag{9}$$

with the local qubit entanglement being propagated throughout the lattice by the unitary streaming operators

$$S_{\Delta\boldsymbol{x},0} = n + e^{\Delta\boldsymbol{x}\partial_{\boldsymbol{x}}}\,\bar{n}, \qquad S_{\Delta\boldsymbol{x},1} = \bar{n} + e^{\Delta\boldsymbol{x}\partial_{\boldsymbol{x}}}\,n, \tag{10}$$

$n = \frac{1}{2}(1-\sigma_z)$ and $\bar{n} = \frac{1}{2}(1+\sigma_z)$ with a shift in the components of ψ along the lattice directions $\pm\Delta\boldsymbol{x}$, respectively. In essence, (10) unitarily shifts just one of these post-collision excited state amplitude probability to the nearest neighbor lattice site $\boldsymbol{x} \pm \Delta\boldsymbol{x}$, respectively. In particular, let us first consider the evolution operator for the γth component of ψ. Our quantum algorithm interleaves the noncommuting collide and stream operators, *i.e.* $[S_{\Delta\boldsymbol{x},\gamma}, C] \neq 0$,

$$I_{x\gamma} = S_{-\Delta\boldsymbol{x},\gamma} C S_{\Delta\boldsymbol{x},\gamma} C \tag{11}$$

where γ is either 0 or 1 corresponding to the streaming of either the α_{01} or α_{10} component of ψ in (9).

One now considers the evolution operator for the γ component of wave function ψ

$$U_\gamma[\Omega(\boldsymbol{x})] = I^2_{x\gamma} exp[-i\varepsilon^2\Omega(\boldsymbol{x})], \tag{12}$$

where Ω will later be specified as a nonlinear potential. ε is a small perturbative parameter. The final quantum map with which we computationally evolve the wave function ψ is

$$\psi(\boldsymbol{x}, t+\Delta t) = U[\Omega(\boldsymbol{x})]\,\psi(\boldsymbol{x},t), \qquad \text{with} \qquad U[\Omega] = U_1\left[\frac{\Omega}{2}\right] U_0\left[\frac{\Omega}{2}\right]. \tag{13}$$

To recover the 1D NLS from this mesoscopic quantum map, one must choose parameters such that the quantum map obeys diffusion ordering, with $\Delta\boldsymbol{x} \sim \varepsilon$, $[\psi(\boldsymbol{x}, t+\Delta t) - \psi(\boldsymbol{x},t)] \to \varepsilon^2\partial_t\psi(\boldsymbol{x},t)$, and contracts the 2-component field ψ to the scalar 1D NLS wave function $\Phi = (1,1)\cdot\psi = \alpha_{01} + \alpha_{10}$ and chooses the nonlinear potential $\Omega = -|\Phi|^2$.

The QLG algorithm is readily extended to the scalar 3D NLS (or commonly called the Gross-Pitaevskii equation in BEC literature): the evolution operator for the γ component is

$$3D: \qquad U_\gamma[\Omega(\boldsymbol{x})] = I^2_{x\gamma} I^2_{y\gamma} I^2_{z\gamma} exp[-i\varepsilon^2\Omega(\boldsymbol{x})]. \tag{14}$$

The extension to spinor superfluids is also straight new 2-qubits $|\psi'\rangle = |q'_1 q'_2\rangle$ for each scalar component of the macroscopic wave function describing the spinor field. The coupling of spinor field components is achieved by suitably defining the nonlinear potential Ω.

A. Successes and Limitations of the QLG with $\sqrt{\text{SWAP}}$ collision operator

The success of the $\sqrt{\text{SWAP}}-QLG$ algorithm has been tested on both scalar 1D NLS soliton collisions, vector (Manakov) 1D NLS inelastic collisions - where exact solutions exist and the conditions under which one has inelastic vector soliton collisions - as well as in turbulence studies of the scalar ($3D$) NLS/GP equation. However, as one pushed into examining spinor-BECs and spin energy spectra for spin turbulence we ran into computational limitations with the $\sqrt{\text{SWAP}}-QLG$ algorithm. Theoretically, we have introduced a "small" parameter $\varepsilon << 1$, and required diffusion ordering $\Delta \boldsymbol{x} \sim \varepsilon$ with $\Delta t \sim \varepsilon^2$ in order to recover the 1D NLS. Numerically, these conditions are met by primarily restricting the amplitude of the qubits. It turns out that this maximum amplitude is dependent on the actual unitary collision operator. In particular, for the unitary $\sqrt{\text{SWAP}}$ collision operator, a "safe" wave function amplitude $|\psi| \sim 0.012$ and a soliton speed ~ 0.033 lattice units/time step. For the 1D NLS the appropriate range of parameters is readily checked since not only do we have the exact 1-soliton solution to the 1D scalar NLS but in soliton-soliton collisions the post-collision solitons retain their origin functional form and speed – the only signature of the soliton-soliton collision is a constant spatially induced phase shift. In the more general case in which the exact solution is not known (like for GP representation of the ground state of the 3D BEC), one has as a necessary condition the conservation of energy since the GP equation is Hamiltonian. For the 1D NLS bright soliton case, the energy integral

$$E = \int dx \left[\left| \frac{\partial \psi}{\partial x}(x,t) \right|^2 - \frac{1}{2}|\psi(x,t)|^4 \right] = \text{Const.} \tag{15}$$

The conservation of the normalization of the wave function (conservation of particle number $\int dx|\psi|^2$) is automatic because of the unitarity of the QLG algorithm.

When the QLG algorithm was extended to simulate the spin-1 BECs it was found that the numerical stability of the algorithm did not permit sufficiently high amplitude wave functions to determine an appropriate spin energy spectrum.

II. ALTERNATE UNITARY COLLISION OPERATOR: DIRAC EQUATION

Yepez [52, 53] developed the first deterministic and unitary QLG algorithm for relativistic Dirac particle dynamics in 3D. He [54] then developed a new unitary QLG algorithm for the relativistic Dirac particle dynamics adding an effective potential as a Lorentz scalar. Here we take the nonrelativistic limit of this unitary Dirac collision operator and extend it to permit a nonlinear potential. This new collision operator C_D, Eq.(16), replaces both the $\sqrt{\text{SWAP}}$ collision operator and the phase rotation used to implement the potential in the old QLG algorithm [56]:

$$C_D = \begin{pmatrix} cos\,\theta(x) & -i\,sin\,\theta(x) \\ -i\,sin\,\theta(x) & cos\,\theta(x) \end{pmatrix}, \tag{16}$$

with

$$\theta(x) = \frac{\pi}{4} - \frac{1}{8}|\psi|^2. \tag{17}$$

We then use the same inter-leavened sequence of unitary collide-stream operators to recover the 1D bright soliton NLS equation. The nonlinear potential $\Omega = -|\psi|^2/8$ is now an integral part of the collision operator and is not just an extra exponential phase factor as in (14).

The most important consequence of using the nonrelativistic unitary Dirac collision operator C_D in the QLG algorithm is that one can now run 1D NLS simulations with amplitudes that are a factor of 20 to 30 greater than that with the $\sqrt{\text{SWAP}}$ unitary collision operator.

In particular, we consider the Dirac-induced unitary collision operator QLG algorithm for soliton maximum amplitudes 0.44 and 0.25 propagating with speed 0.5 lattice units/time step [In our earlier simulations using the $\sqrt{\text{SWAP}}$ QLG algorithm, [56], the safe soliton peak parameters were 0.025, 0.0125 and speed 0.033 lattice units/time step]. The initial solutions are well separated (by about 4000 lattice units on a grid of 6000). The larger soliton always moves to the right while the smaller soliton always moves to the left under periodic boundary conditions. There is significant overlap of the two solitons in their first collision around $t = 40k$, Fig. 1.

After the 15th soliton-soliton collision we see a spatial shift in the location of the solitons due to a collision-induced phase shift, but the solitons retain their exact shape and speed, Fig. 2. The collision-induced spatial shift is greater for the smaller soliton. In Fig. 2 we have chosen the initial snapshot time of $t = 832k$ at which the smaller soliton is at the same spatial location as its initial position at $t = 0$, Fig. 1a. Since the collision-induced phase shift for the larger soliton is less, the spatial position of the larger solution is to the left of its initial position, $t = 0$, Fig. 1a. Hence the soliton collision occurs mainly in the region $x < 0$, Fig. 2.

In Fig. 3 we plot the time development of the collision-induced spatial shift in the larger solition. After every soliton-soliton collision this spatial shift in the larger soliton is +18 lattice units. Since the soliton retains its exact form and speed post-collision there is no spatial shift in-between collisions. Hence the staircase structure in Fig. 3. The Gibbs-like jaggedness during the soliton-soliton collision time is a numerical artifact of the algorithm that simply spits out the location of the maximum in $\psi|$. During the solition-soliton collision this peak location is not necessarily the location of the individual soliton that one has been following before the collision.

The Gibbs-like structures seen in the variation of the total energy (a constant of the time-dependent 1D NLS equation), Fig. 4, is again a numerical artifact because of the grid stencil used to approximate the spatial derivatives in the energy integral, (15). Note that the energy $E < 0$ since the mean nonlinear interaction term in (15) is greater than the mean kinetic energy.

It must be stressed that in the QLG mesoscopic algorithm there is no "knowledge" of the existence of the constant energy integral of 1D NLS. It is only if we have chosen the simulation QLG parameters such that the subsequent moment equations (in this case the 1D NLS equation) arise from diffusion ordering with the existence of the needed theoretical perturbation parameter ε.

A. Limitations on soliton speed

To show some of the limitations on the soliton QLG parameters, we now increase the soliton speed from 0.5 lattice units/time step to 0.75 lattice units/time step but keep the same soliton amplitude peaks of 0.44 and 0.25. There seem no apparent deviations in the snapshots of $|\psi|$ in either pre-collision or post-collision states from their theoretical counterparts. In Fig. 5 one sees $|\psi(x,t)|$ at 6 snapshots starting from time t = 798k, in increments of $\Delta t = 5k$.

However, one starts to see slightly larger fluctuations in the energy constant of the motion (away from the Gibbs-like spikes around the soliton-soliton collisions) for the case of faster speed solitons, Fig. 6. Since the mean kinetic energy of the solitons has increased for these

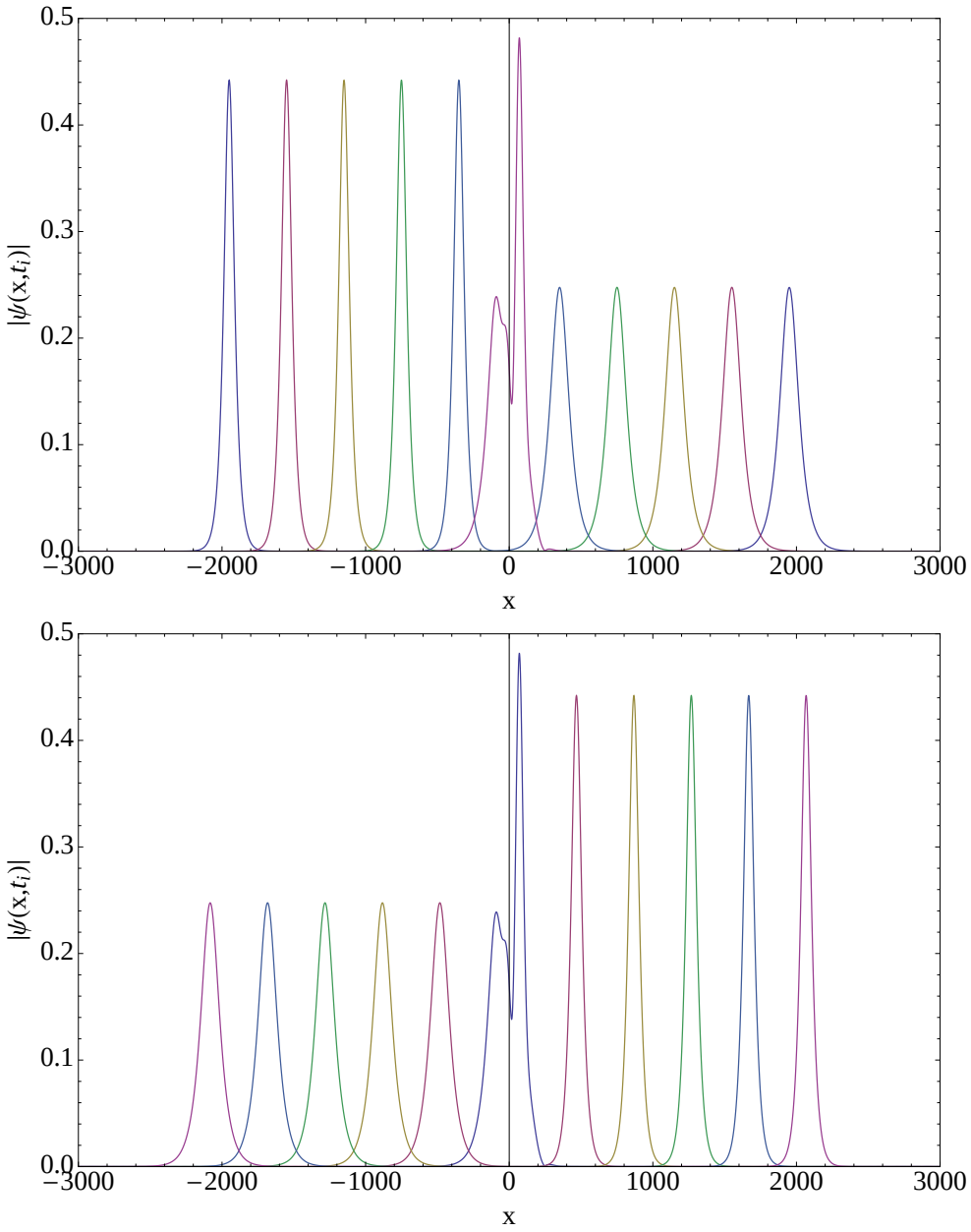

FIG. 1. Snapshots of $|\psi(x,t_i)|$ at time intervals of 8000 ($\Delta t = 8k$) for (*top*) pre-collision and (*bottom*) post-collision soliton motion. Initially the large soliton has its peak around $x \sim -2000$ while the small soliton has its peak around $x \sim +2000$. Color scheme for (*top*): blue (t = 0) → red (t = 8k) → brown (t = 16k) → green (t = 24k) → blue (t = 32k) → red overlap (t = 40k). Color scheme for (*bottom*): blue - overlap (t = 40k) → red (t = 48k) → brown (t = 56k) → green (t = 64k) → blue (t = 72k) → red (t = 80k). The large amplitude soliton always moves to the right while the lower amplitude soliton always moves to the left under periodic boundary conditions. Soliton overlap/collision occurs at $t \sim 40k$. Note that the solitons move with the same amplitude and speed pre- and post-collision.

faster solitons, the total energy E, (15), is now a little less negative.

However, the collision-induced spatial phase shift – that is theoretically a constant away from the soliton-soliton overlap – is the most sensitive to parameter variations, as seen in Fig. 7 over the time interval $800k < t < 920k$ and over all the whole simulation run $0 < t < 10^6$ in Fig. **??**. This should be compared with the corresponding spatial shifts in

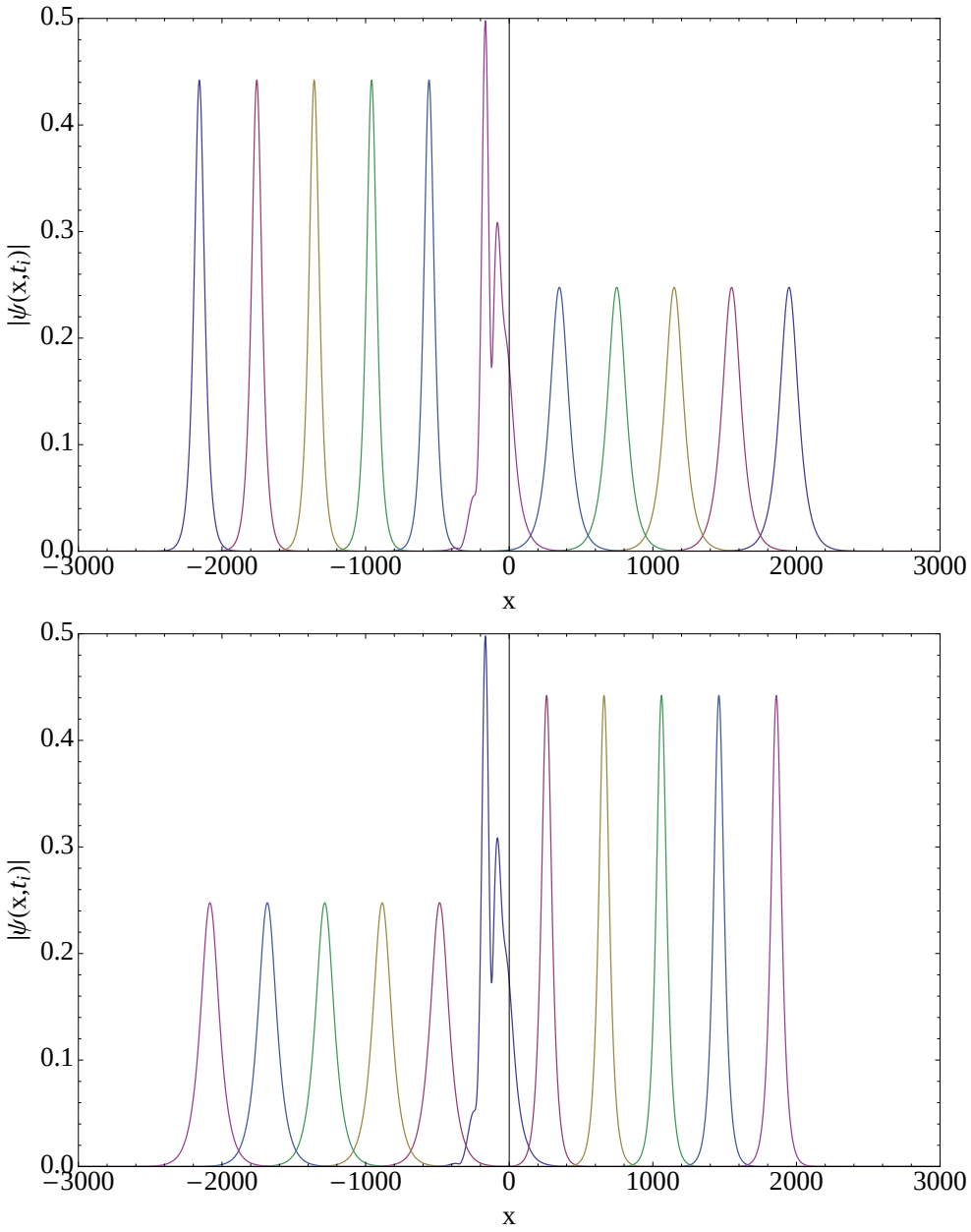

FIG. 2. Snapshots of $|\psi(x,t_i)|$ at time intervals $\Delta t = 8k$ for the post-15th collision. Initial time instant for these 6 snapshots is $t = 832k$ with the large soliton peak around $x \sim -2200$, and the small soliton peak around $x \sim +1950$: (*top*) pre-15th collision and (*bottom*) post-15th collision soliton motion. The large amplitude soliton always moves to the right while the lower amplitude always moves to the left under periodic boundary conditions. Color scheme as explained in Fig. 1.

the large soliton at speed 0.5 lattice units/time step, Fig. 3.

On increasing the soliton speed to 1 lattice unit/time step one still finds that the soliton retain their form and approximate speed as predicted by theory (similar to the plot in Fig. 1), but a closer examination of the energy integral, (15), shows quite large fluctuations while the collision-induced spatial shifts exhibit an unacceptable declination during soliton collisions - indeed much more pronounced than in the case of soliton speed 0.75 lattice units/time step, Fig. 7a.

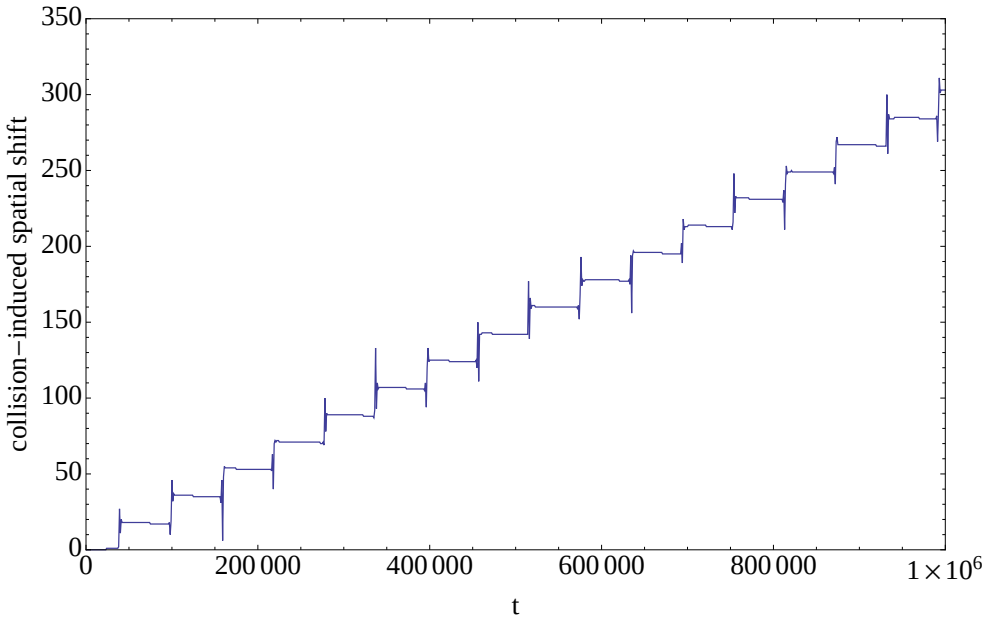

FIG. 3. The time evolution of the collision-induced spatial phase shifts in the large soliton for soliton speed 0.5 lattice units/time step. The spatial shift in-between solition-soliton collisions is basically a constant, as expected theoretically for soliton-soliton collisions of 1D NLS. The Gibbs-like spikes that appear during the soliton-soliton overlap collision is a numerical artifact on the use of the peak in $|\psi|$ during the collision.

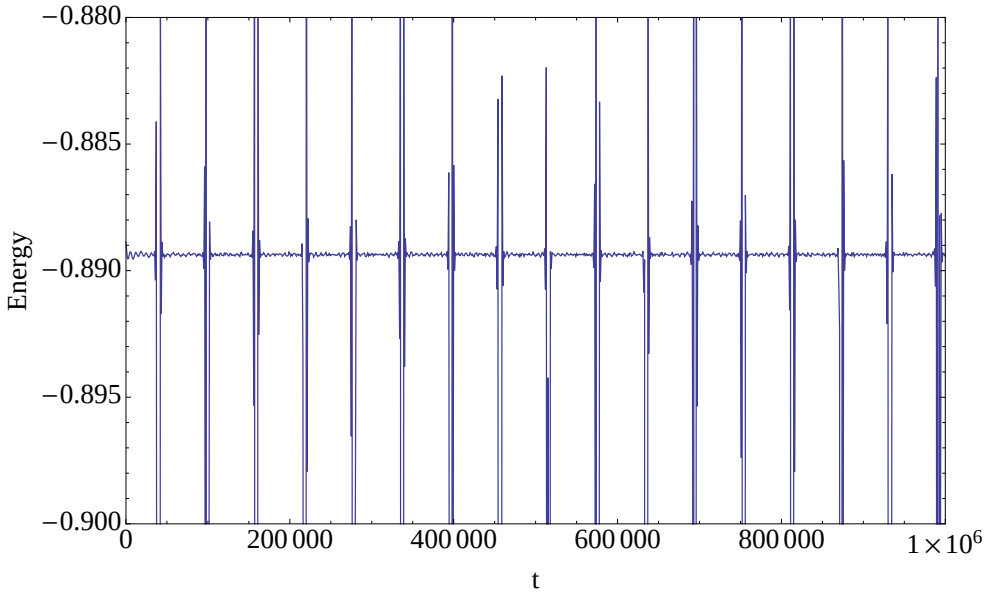

FIG. 4. The time evolution of the energy integral, a constant of the motion of the 1D NLS Hamiltonian system. For the chosen parameters, $E_{cons} = -0.889$. The Gibbs-like spikes that appear during the soliton-soliton overlap collision are numerical artifacts related to the stencil used to calculate Eq.(15).

III. CONCLUSION

We have presented a new quantum lattice gas algorithm for the NLS equation. This approach is based on the quantum lattice gas model the Dirac equation [54] where the

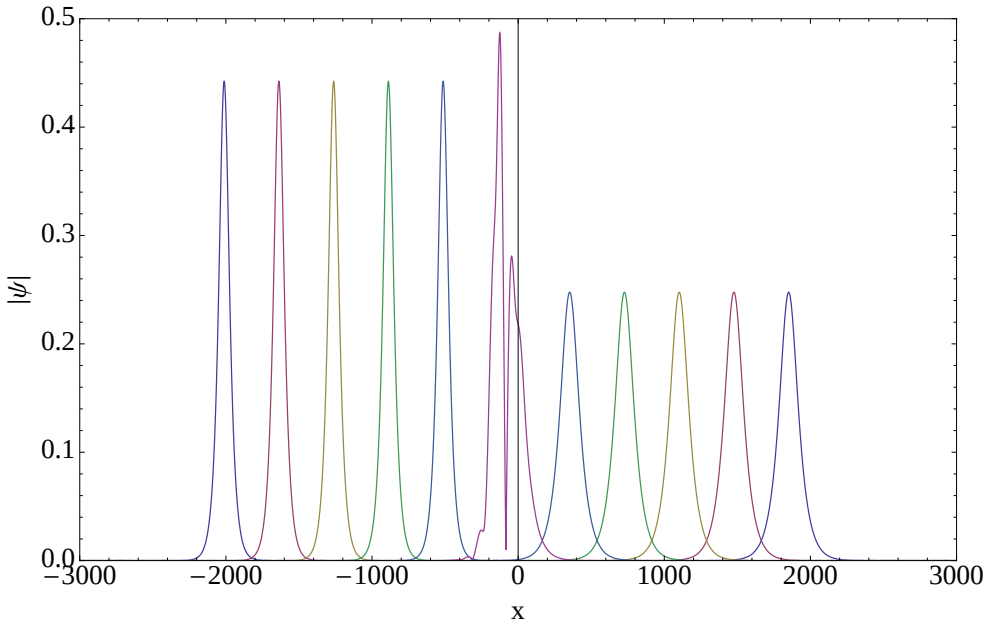

FIG. 5. Snapshots of $|\psi(x,t)|$ in time intervals $\Delta t = 5k$ from t = 798k, after the 20th soliton-soliton collision for the case of higher soliton speed = 0.75 lattice units/time step. The large amplitude soliton (with peak $x \sim -2000$ at t = 798k) is always moving to the right, while the lower amplitude soliton (with peak $x \sim +1850$ at t = 798k) to the left, under periodic boundary conditions. The color scheme as detailed in Fig. 1.

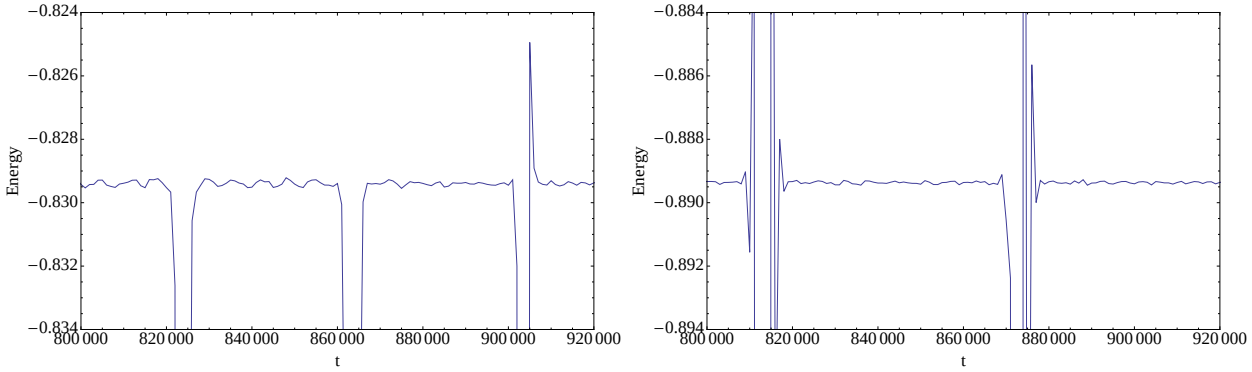

FIG. 6. The fluctuations in the energy integral E, (15), for soliton speed (a) 0.75, and (b) 0.5 lattice units/time step. $E_{(a)} = -0.829$, $E_{(b)} = -0.889$ in the time interval $800k < t < 920k$. As expected the fluctuations are somewhat larger for the higher speed solitons. The Gibbs-like spikes that appear during the soliton-soliton overlap collision are numerical artifacts related to the stencil used to calculate Eq.(15).

particle's mass, a Lorentz invariant scalar quantity, is augmented by an additional scalar quantity that in general is spatially dependent: $m \to m + \delta m(x)$. When the additional mass term is equated to an effective nonlinear potential, i.e. $\delta m(x) = -|\Phi(x)|^2$, we represent an effective potential as a Lorentz scalar quantity. The nonrelativistic limit is then achieved by employing a kinetic energy/potential energy decomposition interleaving scheme that uses a quantum algorithmic protocol of multiple unitary stream and collide operations at each time step. In this way, we can achieve high numerical accuracy even when the coupling constant is large The new QLG algorithm has ben tested against the exactly soluble 1D NLS soliton problem, and we obtain excellent agreement with theory for soliton motion even after 15-20

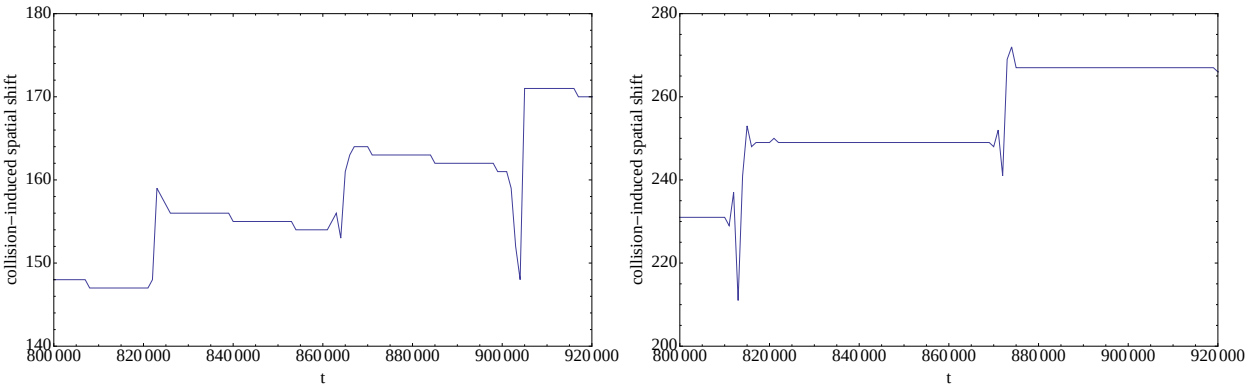

FIG. 7. Fluctuations in the theoretically constant collision-induced spatial phase shifts in the large soliton for soliton speed (a) 0.75, and (b) 0.5 lattice units/time step in the time interval $800k < t < 920k$. As expected the fluctuations are somewhat larger for the higher speed solitons while the actual spatial shifts decrease. The Gibbs-like spikes that appear during the soliton-soliton overlap collision is a numerical artifact on the use of the peak in $|\psi|$ during the collision.

soliton-soliton collisions, with excellent conservation of energy.

IV. ACKNOWLEDGMENTS

This work was supported, in part, by the Air Force Office of Scientific Research and National Science Foundation. While the Dirac QLG computations reported here that mesoscopically represents the 1D NLS equation are performed on a laptop computer, its 3D QLG algorithms have been run on supercomputing facilities at DoD, DoE and NSF. Indeed, we have had timings that scale perfectly on the 786432 cores of the IBM/BlueGene Q *Mira*.

[1] Adriano Barenco, Charles H. Bennett, Richard Cleve, David P. DeVincenzo, Norman H. Margolus, Peter W. Shor, Tycho Sleator, John Smolin, and Harald Weinfurter. Elementary gates for quantum computation. *Physical Review A*, 52(5):3457–3467, 1995.

[2] Richard P. Feynman. There's plenty of room at the bottom. *Caltech Engineering and Science*, February 1960. This is a transcript of Feynman's talk given on December 29, 1959 at the annual meeting of the American Physical Society.

[3] Richard P. Feynman. Simulating physics with computers. *International Journal of Theoretical Physics*, 21(6/7):467–488, 1982.

[4] Paul Benioff. Quantum ballistic evolution in quantum mechanics: Application to quantum computers. *Phys. Rev. A*, 54(2):1106–1123, Aug 1996.

[5] Iwo Bialynicki-Birula. Weyl, Dirac, and Maxwell equations on a lattice as unitary cellular automata. *Phys. Rev. D*, 49(12):6920–6927, Jun 1994.

[6] Bruce M. Boghosian and Washington Taylor. Quantum lattice-gas model for the many-particle schrödinger equation in d dimensions. *Phys. Rev. E*, 57(1):54–66, Jan 1998.

[7] Richard P. Feynman. Geometry of Dirac equ. in 1 dimension. *California Institute of Technology CIT archives*, (13.3), February 1946.

[8] Richard P. Feynman and A.R. Hibbs. *Quantum Mechanics and Path Integrals*. McGraw-Hill, 1965. Problem 2-6 on page 34.

[9] Gerard 't Hooft. Equivalence relations between deterministic and quantum mechanical systems. *J. Stat. Phys.*, 53(1-2):323–344, Mar 1988.

[10] Gerard 't Hooft. Quantum mechanical behaviour in a deterministic model. *Found. Phys. Lett.*, 10(2):105–111, Apr 1997.
[11] David A. Meyer. Quantum mechanics of lattice gas automata: One-particle plane waves and potentials. *Phys. Rev. E*, 55(5):5261–5269, May 1997.
[12] G.V. Riazanov. The Feynman path integral for the Dirac equation. *Soviet Physics JETP*, 6 (33)(6):7 pages, June 1958.
[13] Jeffrey Yepez. New world vistas: New models of computation, lattice based quantum computation. *USAF Technical Report*, (DTIC ADA421712), 1996.
[14] Jeffrey Yepez. Short introduction to quantum computation. *Proceedings of the 1996 AFOSR Meeting of Computational and Applied Mathematics*, USAF Technical Report ADA434366 Air Force Phillips Laboratory, 1996.
[15] Jeffrey Yepez. Lattice gas dynamics: Volume III Quantum algorithms for computational physics. Technical Report AFRL-VS-HA-TR-2006-1143, Air Force Research Laboratory, AFRL/RV Hanscom AFB, MA 01731, January 2007. DTIC ADA474659.
[16] F. Fillion-Gourdeau, H. J. Herrmann, M. Mendoza, S. Palpacelli and S. Succi Formal analogy between the Dirac equation in its Majorana form and the discrete-velocity version of the Boltzmann kinetic equation *Phys. Rev. Lett.*, 113:160602, 2013.
[17] S. Succi and R. Benzi Lattice Boltzmann equation for quantum mechanics *Physica D*, 69:327, 1993.
[18] S. Palpacelli and S. Succi The quantum lattice Boltzmann equation: recent developments *Comm. in Comp. Phys.*, 4:980, 2008.
[19] P. J. Dellar, D. Lapitski, S. Palpacelli and S. Succi Isotropy of three-dimensional quantum lattice Boltzmann schemes *Phys. Rev. E*, 83:046706, 2011.
[20] Y. Kawaguchi and M. Ueda Spinor Bose-Einstein condensates. *Physics Reports* 520:253-381, 2012.
[21] Jeffrey Yepez, George Vahala, and Linda Vahala. Vortex-antivortex pair in a Bose-Einstein condensate. *Euro. Phys. J. Special Topics*, 171:9–14, 2009.
[22] Jeffrey Yepez, George Vahala, Linda Vahala, and Min Soe. Superfluid turbulence from quantum kelvin wave to classical kolmogorov cascades. *Physical Review Letters*, 103(8):084501, 2009.
[23] MH Anderson, JR Ensher, MR Matthews, CE Wieman, and EA Cornell. Observation of bose-einstein condensation in a dilute atomic vapor. *Science*, 269(5221):198–201, 1995.
[24] K. B. Davis, M. O. Mewes, M. R. Andrews, N. J. van Druten, D. S. Durfee, D. M. Kurn, and W. Ketterle. Bose-einstein condensation in a gas of sodium atoms. *Phys. Rev. Lett.*, 75(22):3969–3973, Nov 1995.
[25] M.-O. Mewes, M. R. Andrews, N. J. van Druten, D. M. Kurn, D. S. Durfee, and W. Ketterle. Bose-einstein condensation in a tightly confining dc magnetic trap. *Phys. Rev. Lett.*, 77(3):416–419, Jul 1996.
[26] W Ketterle, M W. Zwierlein, and Societa italiana di fisica. Making, probing and understanding ultracold fermi gases? page 176, Jan 2008.
[27] E. P. Gross. Hydrodynamics of a superfluid condensate. *J.Math.Phys.*, 4(2):195–207, Feb 1963.
[28] L. P. Pitaevskii. Vortex lines in an imperfect Bose gas. *Soviet Phys. JETP*, 13(2):451–454, Aug 1961.
[29] N. Andersson, G. L. Comer, and D. Langlois. Oscillations of general relativistic superfluid neutron stars. *Phys. Rev. D*, 66(10):104002, Nov 2002.
[30] G. L. Comer, David Langlois, and Lap Ming Lin. Quasinormal modes of general relativistic superfluid neutron stars. *Phys. Rev. D*, 60(10):104025, Oct 1999.
[31] Mikhail E. Gusakov. Bulk viscosity of superfluid neutron stars. *Physical Review D (Particles, Fields, Gravitation, and Cosmology)*, 76(8):083001, 2007.
[32] Lap-Ming Lin, N. Andersson, and G. L. Comer. Oscillations of general relativistic multifluid/multilayer compact stars. *Physical Review D (Particles, Fields, Gravitation, and Cosmology)*, 78(8):083008, 2008.
[33] Lee Lindblom and Gregory Mendell. r-modes in superfluid neutron stars. *Phys. Rev. D*, 61(10):104003, Apr 2000.

[34] Shijun Yoshida and Umin Lee. r-modes in relativistic superfluid stars. *Phys. Rev. D*, 67(12):124019, Jun 2003.
[35] Stefano Giorgini, Lev P. Pitaevskii, and Sandro Stringari. Theory of ultracold atomic fermi gases. *Rev. Mod. Phys.*, 80(4):1215–1274, Oct 2008.
[36] C. A. Regal, M. Greiner, and D. S. Jin. Observation of resonance condensation of fermionic atom pairs. *Phys. Rev. Lett.*, 92(4):040403, Jan 2004.
[37] George Vahala, Jeffrey Yepez, and Linda Vahala. Quantum lattice gas algorithm for quantum turbulence and vortex reconnection in the Gross-Pitaevskii equation. In Eric J. Donkor, Andrew R. Pirich, and Howard E. Brandt, editors, *Quantum information theory*, volume 6976, page 69760U. SPIE, 2008.
[38] Jeffrey Yepez, George Vahala, and Linda Vahala. Twisting of filamentary vortex solitons demarcated by fast Poincare recursion. volume 7342, page 73420M. SPIE, 2009.
[39] Immanuel Bloch, Jean Dalibard, and Wilhelm Zwerger. Many-body physics with ultracold gases. *Rev. Mod. Phys.*, 80(3):885–964, Jul 2008.
[40] R. P. Feynman. *Progress in Low Temperature Physics*, volume I. North-Holland, Amsterdam, 1955.
[41] Russell J. Donnelly. *Quantized vortices in helium II.* Cambridge University Press, Cambridge [England]; New York, 1991.
[42] Carlo F. Barenghi. Is the reynolds number infinite in superfluid turbulence? *Physica D: Nonlinear Phenomena*, 237(14-17):2195 – 2202, 2008. Euler Equations: 250 Years On - Proceedings of an international conference.
[43] G. Boffetta, A. Celani, D. Dezzani, J. Laurie, and S. Nazarenko. Double kelvin wave cascade in superuid helium. 2008.
[44] Evgeny Kozik and Boris Svistunov.. 40 Kelvin-wave cascade and decay of superfluid turbulence. *Phys. Rev. Lett.*, 92(3):035301, Jan 2004.
[45] Evgeny Kozik and Boris Svistunov. Kolmogorov and kelvin-wave cascades of superfluid turbulence at t = 0: What lies between. *Physical Review B (Condensed Matter and Materials Physics)*, 77(6):060502, 2008.
[46] Victor S. L'vov, Sergei V. Nazarenko, and Oleksii Rudenko. Bottleneck crossover between classical and quantum superfluid turbulence. *Physical Review B (Condensed Matter and Materials Physics)*, 76(2):024520, 2007.
[47] Boris V. Svistunov. Superfluid turbulence in the low-temperature limit. *Phys. Rev. B*, 52(5):3647–3653, Aug 1995.
[48] C. Nore, M. Abid, and M. E. Brachet. Decaying kolmogorov turbulence in a model of superflow. *Physics of Fluids*, 9(9):2644–2669, 1997.
[49] SZ Alamri, AJ Youd, and CF Barenghi. Reconnection of superfluid vortex bundles. *Phys. Rev. Lett.*, 101(21):215302, 2008.
[50] D Kivotides. Coherent structure formation in turbulent thermal superfluids. *Phys. Rev. Lett.*, 96(17):175301, 2006.
[51] Jeffrey Yepez. k^{-3} superfluid spectrum of highly curved interacting quantum vortices. *arxiv:1002.4380v1*, quant-ph, 2009.
[52] Jeffrey Yepez. arXiv:quant-ph/0210093, 2003.
[53] Jeffrey Yepez. *Quantum Information Processing* **4**(6), 471 2005.
[54] Jeffrey Yepez. Quantum lattice gas model of Dirac particles in 1+1 dimensions. *arxiv:1307.3595v1*, quant-ph, 2013.
[55] Naoya Suzuki, Hiromitsu Takeuchi, Kenichi Kasamatsu, Makoto Tsubota, and Hiroki Saito. Crossover between kelvin-helmholtz and counter-superflow instabilities in two-component bose-einstein condensates. *Phys. Rev. A*, 82:063604, Dec 2010.
[56] George Vahala, Jeffrey Yepez, and Linda Vahala Quantum lattice gas representation of some classical solitons. *Phys. Lett. A*, 310:187, 2003.